Journal Name

ARTICLE

Supporting Information

Improving organic tandem solar cells based on water-processed nanoparticles by quantitative 3D nanoimaging~~Water-processed organic tandem solar cells improved by quantitative 3D nanoimaging~~

*Emil B. L. Pedersen, Dechan Angmo, Henrik F. Dam, Karl T. S. Thydén, Thomas R. Andersen, Eirik T. B. Skjønsfjell, Frederik C. Krebs, Mirko Holler, Ana Diaz, Manuel Guizar-Sicairos, Dag W. Breiby and Jens W. Andreasen**

S.1. Spatial resolution by Fourier shell correlation

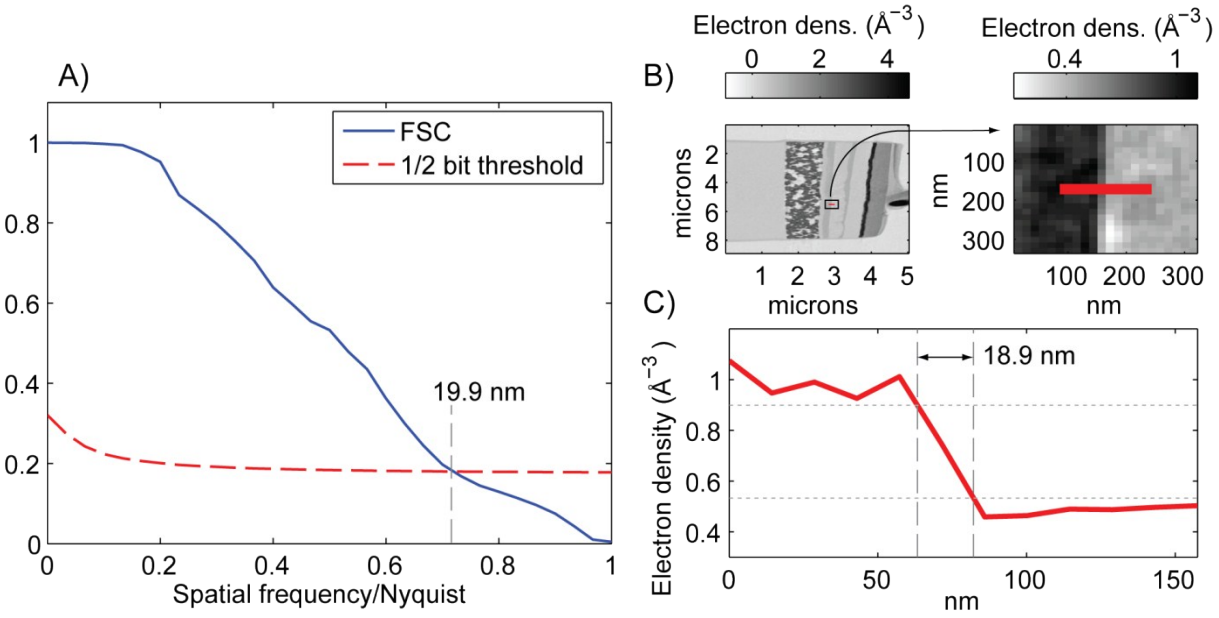

Figure S1: A) Fourier shell correlation (FSC) calculated for a central part of the tomographic data shown in the in main article. The 0.5 bit threshold intersects at 0.72 spatial frequency / Nyquist limit which with a Nyquist limit of 14.3 nm corresponding to 14.3 nm / 0.72 = 19.9 nm isotropic half period spatial resolution. B) Schematics of line scan shown in C) which yield 18.9 nm spatial resolution with the 10%-90% criterion.

The sample was measured at 470 projections that were reconstructed to a voxel side length at a half-period Nyquist limit of 14.3 nm. The resolution of the 3D dataset obtained by ptychographic tomography was estimated

by Fourier shell correlation (FSC),[19,22] using two tomograms each computed from half of the projections. In Figure S1 we show in blue the computed FSC as a function of the spatial frequency on a Nyquist sampling scale. This curve can be compared with an analytically calculated threshold curve for a given signal-to-noise ratio, shown in Figure S1 with a dashed red line. The point at which the threshold curve intersects the FSC curve determines the spatial resolution, which in this case is 0.72 spatial frequency / Nyquist limit and corresponds to 19.9 nm. We note that this resolution estimation could be pessimistic because the correlation is computed from tomograms with only half of the projections in each. The coarser angular sampling can reduce the FSC at high spatial frequencies and provide a low estimate of the resolution, and as seen on figure S1 the line scan yields a slightly better spatial resolution of 18.9 nm.

S.2. Partial volume simulations

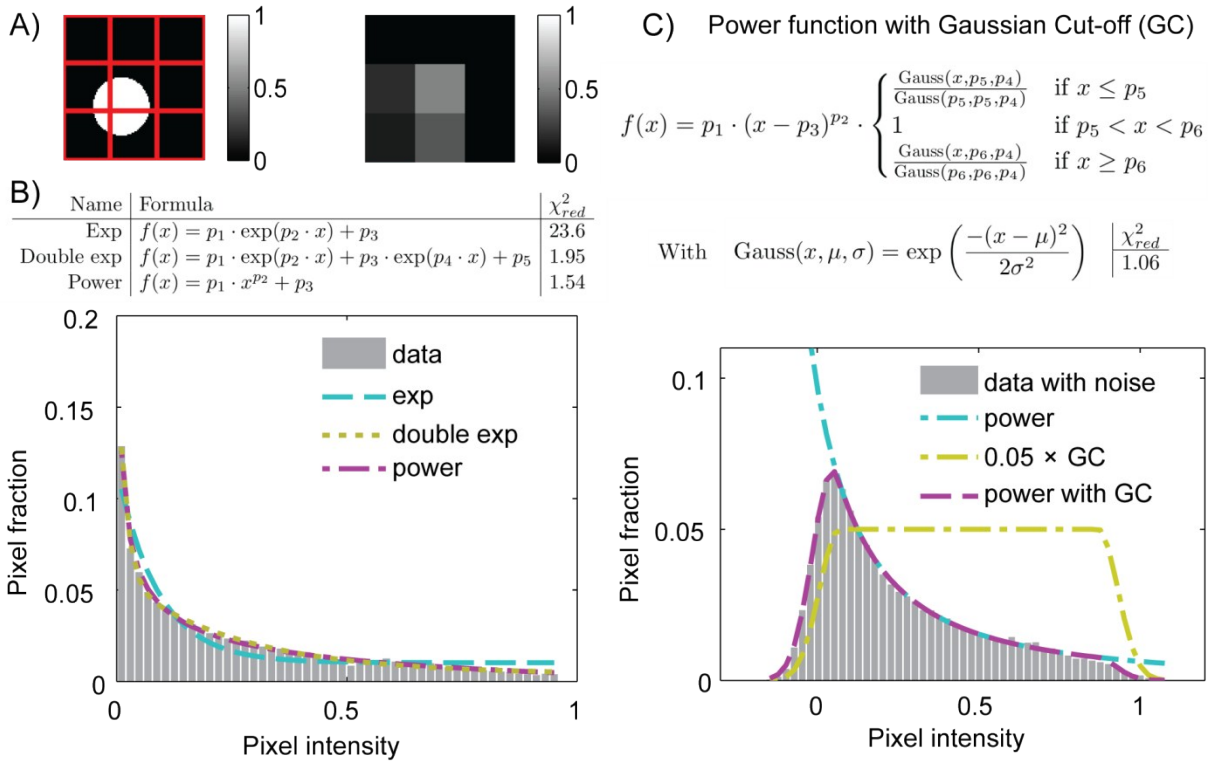

Figure S2: A) Illustration of simulation where sub-resolution cylinders (white =1, radius of 0.6 pixels) are randomly placed within a different medium (black = 0). The observed intensities due to partial volume effects are evaluated for 10^4 cylinders exemplified in the right figure. B) Resulting intensity histograms from the simulations described in A) are fitted with different functions. The goodness of fit is evaluated by reduced chi square assuming Poisson statistics and the power function is found to best match the distribution. C) The simulations are expanded to include Gaussian noise on the pixel intensities (σ = 0.05). To fit the new distribution the power function is multiplied with a step function with Gaussian Cut-offs (GC). The resulting fit yields a reduced χ^2 of about 1, and is shown along with two components of the fit: the power law function and the GC.

In a simulation carried out to calibrate the fit functions, a cylinder with diameter below the resolution was placed in a different medium, and the resulting partial volumes were calculated as shown in figure S2. 10^4 cylinders (r = 0.6 px) were randomly placed within the center pixel as illustrated in figure S2A using a uniform probability distribution without loss of generality due to the system symmetry. The resulting intensity distribution was fitted with different mathematical fit functions and found to be best described by a power law as shown in figure S2B. In real data sets the voxels will have noise due to experimental uncertainties, which is included in the simulation

as Gaussian perturbations of the pixel intensities (μ = 0, σ = 0.05). The new resulting distribution of the simulated noisy data is fitted with a product of a power function and a step function with Gaussian Cut-off (GC) as shown in figure S2C. The function is evaluated to be a good description of partial volumes effects like sub-resolution features based on the reduced χ^2 value near unity.

S.3 Markov field segmentation

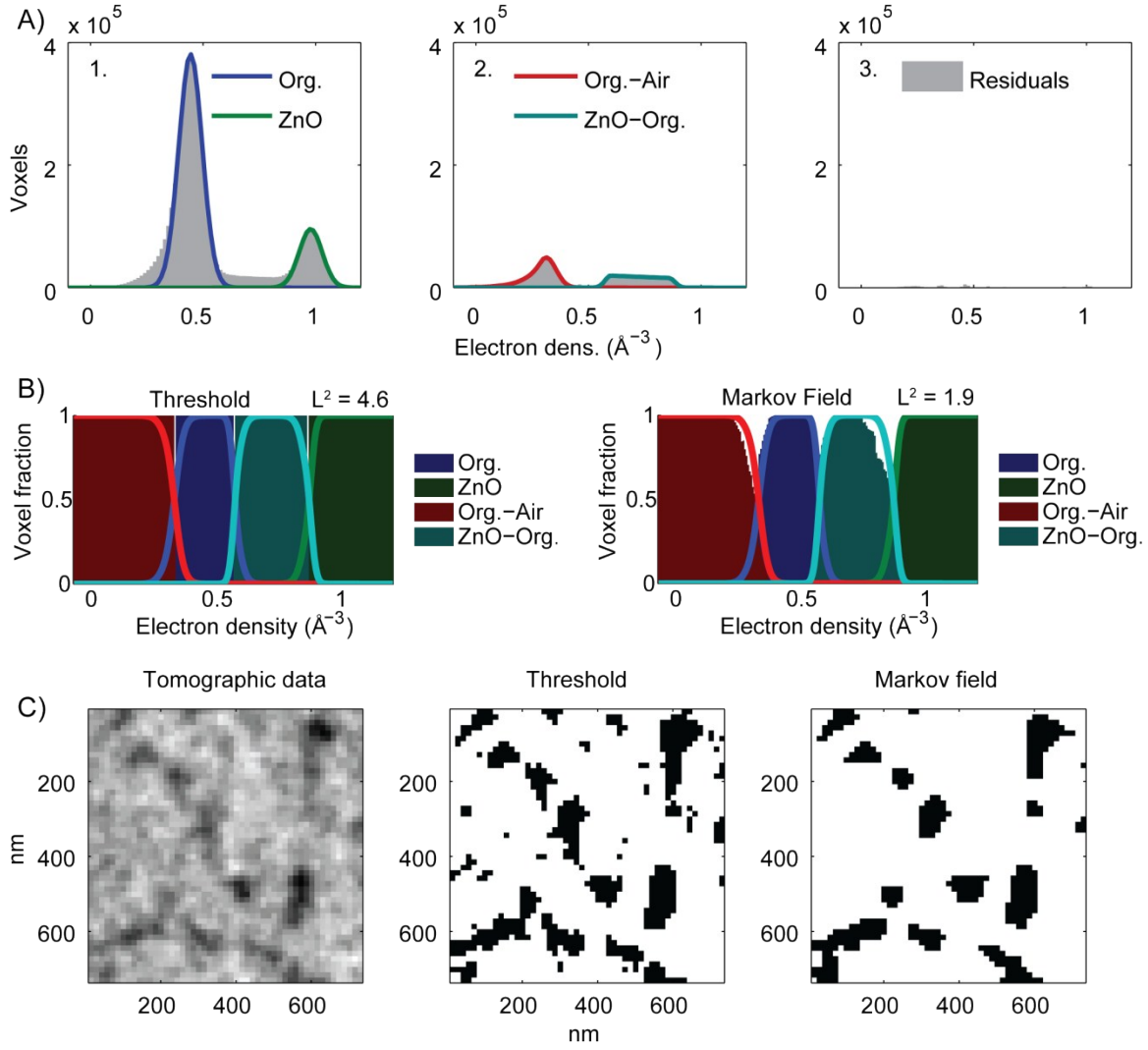

Figure S3: A) Electron density histograms from a subset of the tomogram are fitted with (1) Gaussian functions for pure materials and (2) power functions with Gaussian cut-offs for material mixtures as described in S2, after subtracting the Gaussian fits in (1) from the histogram. With insignificant residuals (3) the data are described solely by these 4 functions carrying strict physical meaning. B) The fitted functions from A) are converted to relative amount of voxels for each electron density. These functions are compared to the actual fraction of voxel being segmented into the given label at the given electron density. The lines represent the fits in A) and the ~~colored~~coloured areas the actual segmentation in the tomogram. Measured by the L^2 norm the distance of Markov fields segmentation in only 40% the distance of threshold segmentation, Markov fields segmentation thus getting closer to true physical functions in A). C) Organic material (Landfester particles) with volumes containing air. The tomographic data is illustrated to the left and the two types of segmentation are shown to

the right. Note the Markov field is implemented in 3D and uses all neighbors, therefore also taking voxels out of the shown plane into account. The Markov field greatly reduces the noise present in the threshold segmentation.

The nearest neighbors were included in the segmentation by an α-expanded Markov field since it improves the segmentation and thereby more easily justifies the physical interpretations as illustrated in figure S3. The energy function that the Markov function minimizes is

$$E(f) = -\sum_{i \in C_1} \alpha_i f_i - \sum_{(i,j) \in C_2} \beta_{ij} f_i f_j$$

Here C_x is the *x*-clique, *f* is the segmentation label, and α and β are weights for the 1- and 2- cliques, respectively. In practice the α parameters were set to 1, and the β parameters were optimized by performing full segmentation combined with a pattern search algorithm to minimize the distance to the describing functions presented for a sub section of the tomogram in figure S3. In this example the functions give: Org.-Air(0.35 Å^{-3}) ~ $3.4 \cdot 10^4$ voxels and Org.(0.35 Å^{-3}) ~ $7.5 \cdot 10^4$ voxels, so the expected voxel fraction at 0.35 Å^{-3} electron density is ~0.3 for Org.-Air and ~0.7 for Org. material. The threshold segmentation gives Org.-Air(0.35 Å^{-3}) = 0 voxels and Org.(0.35 Å^{-3}) = $1.09 \cdot 10^5$ voxels thus reaching voxel fraction of 0 for Org.-Air and 1 for Org. material and residuals of 0.3 compared to their respective functions. The actual Markov segmentation was performed using a graph cut algorithm based on [Y. Boykov and V. Kolmogorov, *IEEE Trans. Pattern Anal. Mach. Intell.*, 2004, **26**, 1124–37].

S.4. Materials, fabrication, and photovoltaic characterization of tandem solar cells

Materials: Flextrode substrate that is comprised of Ag-grids/PEDOT:PSS/ZnO on PET substrate produced in a roll-to-roll machinery using Flexographic printing (Ag grids), rotary screen printing (PEDOT:PSS) and slot-die coating (ZnO)1,2 was acquired from InfinityPV (www.infinitypv.com). ZnO nanoparticle solution was also obtained from infinityPV in acetone with a concentration of 56 mg ml-1. P3MHOCT and PDTSBT-F:PCBM were synthesized in house.3,4 [60]PCBM with 99% purity was obtained from Merck. All organic solvents were of technical grade and purchased from Sigma-Aldrich with 99% purity. PEDOT:PSS Clevious P VP AL 4083 and PEDOT:PSS Clevious F010 were purchased from Heraeus Materials GmbH. Thermally curable Ag paste (PV 410) for the top silver electrode was purchased from DuPont. Sodium Dodecyl Sulfate (SDS) was purchased from Sigma Aldrich.

Fabrication: P3MHOCT and PCBM were mixed in a ratio of 1:1 in chloroform and processed into nanoparticles using the Landfester method[5] with Sodium Dodecyl Sulfate (SDS) as surfactant. The ink concentration was increased to 60 mg/mL by centrifugation. PDTSBT-F:PCBM was mixed in 1:1.5 ratio by weight and dissolved in chloroform with a solid concentration of 35 mg mL^{-1} . The mixture was heated on a hot plate at 70^{o}C for 2-3 hours to achieve complete dissolution prior to the fabrication of the solar cells. Solar cells with inverted geometry were coated on Flextrode substrate. 1 m of these substrates were cut from the roll of Flextrode and subsequent device stacks were fabricated using a laboratory roll-coater.[6] Firstly, the P3MHOCT nanoparticle active ink was slot-die coated at a speed of 1.30 m min^{-1} and a flow-rate of 0.220 ml min^{-1} and a substrate temperature of 100 ^{o}C thus resulting in a wet-layer thickness of 17 µm and an estimated dry layer thickness of ~920 nm. On top of this layer, the recombination layer was printed through slot-die coating. The recombination layer comprised three layers.[7,8] Briefly, the first layer is a PEDOT:PSS layer based on Clevios F-010 diluted with isopropanol (IPA) in 1:4 *vol/vol* which is used as a wetting-agent/compatibilizer. This layer was slot-die coated at a speed of 1.30 m min^{-1} and flow rate of 0.10 ml min^{-1}. The second PEDOT:PSS layer consists of Clevios P VP AL 4083 diluted with IPA in 1:1 *v/v* which was slot-die coated on top of the compatibilizer layer at the same speed and a flow rate of 0.30 mL $min^{-1.}$

Finally, the recombination layer was completed by slot-die coating ZnO at a speed of 2 m min^{-1} and a flow-rate of 0.08 mL min^{-1} resulting in a dry layer thickness of 40 nm. All three layers in the recombination layer were coated at 60 °C.

On top of the recombination layer, the second active layer based on PDTSBT-F:PCBM was slot-die coated at a speed of 1.30 m min^{-1} and 0.120 mL min^{-1} at 60 °C resulting in a wet layer thickness of 9 µm and a dry layer thickness of 247 nm. The PEDOT:PSS back electrode was fabricated in a three step coating procedure as described elsewhere.[8] Finally, the Ag grid was flexo printed. All devices were annealed at 110 °C for 5 minutes post fabrication to achieve curing of flexo printed Ag grid while also annealing the photoactive layer. Individual cells were cut from the each stripe, and randomly characterized for photovoltaic properties. The device area was ~1 cm^2.

Photovoltaic Characterization

IV-characteristics were measured under 1000 W m^{-2} AM 1.5G condition using a Keithley 2400 source meter and illumination was provided by a KHS SolarConstant 575 solar simulator (Steuernagel Lichtteknik) which was calibrated with a reference photodiode to 100 mW cm^{-2} AM1.5G. Mismatch factors were not taken into account.

Table S1. Device photovoltaic performance with double sided illumination[1] is shown for the investigated tandem cells. All devices correspond to those reported in Table 1. BHJ_1 = PDTSBT-F:PCBM, BHJ_3 = P3MHOCT:PCBM and NP_3 = P3MHOCT:PCBM as Landfester particles.

	V_{oc} (V)	J_{sc} (mA cm^{-2})	FF (%)	PCE (%)
Tandem BHJ_1 – NP_3	0.34	1.16	27.15	0.11
Tandem BHJ_1 – NP_3+ PCBM	0.60	0.68	29.18	0.07
Tandem BHJ_1 – NP_3+ BHJ_3	1.02	0.17	25.35	0.04

1. D. Angmo, S. A. Gevorgyan, T. T. Larsen-Olsen, R. R. Søndergaard, M. Hösel, R. Gupta, G. U. Kulkarni, F. C. Krebs, Organic Electronics, 2013, 14(3), 984-994.
2. M. Hösel, R. R. Søndergaard, M. Jørgensen, F. C. Krebs, Energy Technology, 2013, 1, 102-107.

3. J. E. Carlé , M. Helgesen , M. V. Madsen , E. Bundgaard , F. C. Krebs , J. Mater. Chem. C 2014 , 2 , 1290 .
4. M. Bjerring, J. S. Nielsen, A. Siu, N. C. Nielsen, F.C. Krebs. Solar Energy Materials and Solar Cells 92.7 (2008): 772-784.
5. T. Kietzke, D. Neher, M. Kumke, R. Montenegro, K. Landfester, and U. Scherf, Macromolecules, 2004, 37, 4882–4890.
6. H. F. Dam, F.C. Krebs, Sol. Energy Mater. Sol. Cells, 2012, 97, 191-196.
7. T. R. Andersen, H. F. Dam, B. Andreasen, M. Hösel, M. V. Madsen, S. A. Gevorgyan, R. R. Søndergaard, M. Jørgensen, and F. C. Krebs, Sol. Energy Mater. Sol. Cells, 2014, 120, 735–743.
8. D. Angmo, H. F. Dam, T. R. Andersen, N. K. Zawacka, M. V. Madsen, J. Stubager, F. Livi, R. Gupta, M. Helgesen, J. E. Carlé, Energy Technology. 2014, 2(7), 651-659